Single-Molecule Chemistry and Vibrational Spectroscopy: Pyridine and Benzene on Cu(001)

L. J. Lauhon and W. Ho*

Laboratory of Atomic and Solid State Physics and Cornell Center for Materials Research, Cornell University, Ithaca, New York 14853

Received: June 2, 1999; In Final Form: August 27, 1999

A variable-temperature scanning tunneling microscope (STM) was used to perform single-molecule chemistry and vibrational spectroscopy on benzene (C_6H_6), pyridine (C_5H_5N), and their isotopes adsorbed on Cu(001) at 8 K. Inelastic electron tunneling spectra taken with the STM (STM-IETS) showed a C−H stretch mode for pyridine but not for benzene. Individual pyridine and benzene molecules were dissociated by tunneling electrons. The fragments of each parent molecule were imaged and the vibrational spectra recorded. A C−H stretch mode was detected by STM-IETS for the fragments of both molecules. The detection of a C−H stretch mode in the benzene fragment is attributed to a change in bonding geometry with respect to the parent. The images and spectroscopic data are consistent with the production of C_5H_4N and C_6H_4 in the dissociation of pyridine and benzene, respectively.

Introduction

The scanning tunneling microscope (STM) is perhaps best known for producing real-space images of molecules adsorbed on solid surfaces with a spatial resolution that can permit the determination of the adsorption site and geometry.[1] In one case, three types of STM images were seen for benzene adsorbed on Pt(111).[2] Comparison with calculated images led to the identification of three types of adsorptions sites,[3] thus demonstrating the sensitivity of STM as a tool for correlating electronic and spatial structure. The STM is also capable of inducing chemical reactions on the atomic scale because of the geometric confinement of the energetic tunneling electrons.[4] In one example of a unimolecular reaction, the STM was used to transfer energy from tunneling electrons to a single oxygen molecule on the Pt(111) surface.[5] The tunneling electrons induced electronic and vibrational excitations which led to dissociation. Comparison with photodissociation and thermal dissociation in the same system contributed to the understanding of the microscopic mechanisms of chemical reactions. Yet another capability of the STM has recently been established: single-molecule vibrational spectroscopy. The vibrational signature of a single bond can be detected by performing inelastic electron tunneling spectroscopy in the junction of an STM (STM-IETS).[6] The vibrational spectra of chemisorbed molecules often show shifts from the gas phase which carry information about the nature of the molecule−surface bond. Further shifts may be induced by chemical transformation.

When the STM techniques of imaging, chemical manipulation, and vibrational spectroscopy are brought to bear on an adsorption system, significant understanding can be gained. The system we have chosen for study is benzene and pyridine on Cu(001) at 8 K. A variable-temperature STM was used to perform STM-IETS on pyridine, benzene, and their dissociation products produced by energetic tunneling electrons. The C−H stretch mode was identified for pyridine, a pyridine fragment, and a benzene fragment. Isotopes were used to confirm the peak identifications, and acetylene spectra were taken for comparison with previous studies. The images and vibrational spectra of the molecular fragments lend clues to their identities. The results of vibrational spectroscopy have implications for the practical application and theoretical development of STM-IETS. The dissociation and imaging results present interesting opportunities for electronic structure calculations and STM image simulations to be compared with experimental data.

Experimental Section

Experiments were performed using a home-built variable-temperature STM housed in an ultrahigh vacuum chamber with a base pressure of 2×10^{-11} Torr.[7] The Cu(001) sample was prepared by 1 keV neon ion sputtering followed by annealing at 800 K. Polycrystalline tungsten tips were prepared *in situ* by self-sputtering and annealing. Adsorbates were introduced into the chamber via a capillary array doser attached to a variable-leak valve. Room temperature liquid sources of pyridine and benzene were used after purification by repeated freeze−pump−thaw cycles. The dosing and all experiments described herein took place at 8 K.

Pyridine Imaging. A constant-current STM image of pyridine, pyridine-d_5, and acetylene-d_1 is shown in Figure la. Pyridine appears as a protrusion on the Cu(001) surface under typical imaging conditions while acetylene appears as a depression. Acetylene binds at four-fold hollow sites with the molecular axis parallel to the [100] or [010] axis.[6] Pyridine binds to copper predominantly through the nitrogen lone pair electrons.[8] In the case of Cu(110), the molecular plane is perpendicular to the surface and the [1$\bar{1}$0] close-packed rows.[9,10] For Cu(111), the angle between the surface and the molecular plane is 70°.[9] Data for pyridine on Cu(001) are consistent with vertically oriented pyridine.[10] The apparent height of pyridine in Figure la is 1.9 Å. Pyridine is of the same apparent height on Cu(110) in STM images taken under the same conditions.[11] Despite the C_{2v} symmetry of the vertically oriented molecule, no azimuthal asymmetry was observed in any pyridine image which could be ascribed to the molecule. Multiple observations

* Corresponding author. E-mail address: wilsonho@ccmr.cornell.edu.

10.1021/jp991768c CCC: $19.00
Published on Web 11/03/1999

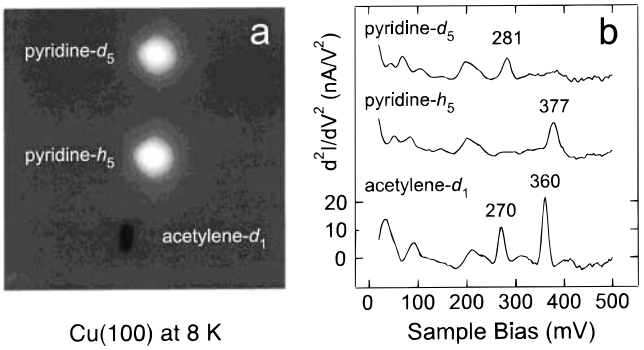

Figure 1. (a) 60 × 60 Å constant-current STM image of pyridine-d_5, pyridine, and acetylene-d_1, taken at 1 nA and 0.25 V sample bias. (b) d^2I/dV^2 for the molecules of (a) taken at a gap resistance of 250 MΩ (1 nA, 0.25 V) with a 7 mV bias modulation at 200 Hz. A background spectrum taken over the bare copper surface has been subtracted from each of the molecular spectra. The spectra are averages of 165 scans from 0 to 500 mV and back down to 0 mV in 2.5 mV increments. Each scan takes 2 min.

with different tips lead to the conclusion that, under the imaging conditions used in this study, the symmetry of the tip determines the symmetry of the pyridine image.

Pyridine IETS. The STM implementation of IETS has been described previously in detail.[6,7] Briefly, the tip is positioned over the molecule to be studied by locating the local maximum or minimum in height using an iterative tracking routine. With the feedback off, the sample bias voltage is ramped over the range of vibrational peaks while a sinusoidal bias modulation is superimposed.[12] When the energy of the tunneling electrons is sufficient to excite a "tunneling-active" vibrational mode of the molecule, the conductance increases because of the onset of an inelastic tunneling channel. The derivative of the conductance exhibits a peak at the molecular vibrational energy $\hbar w = eV_{bias}$. The conductance $\sigma = dI/dV$ and its derivative $d\sigma/dV = d^2I/dV^2$ are proportional to the first and second harmonics of the tunneling current which are measured with a lock-in amplifier. $I - V$ measurements were taken to determine the proportionality constants. For comparison, background spectra were taken over clean areas of the surface.

STM-IETS spectra for pyridine, pyridine-d_5, and acetylene-d_1 are shown in Figure lb. C−H and C−D stretch modes of pyridine and pyridine-d_5 are identified at 377 and 281 meV, respectively. Reflection−absorption infrared spectroscopy (RAIRS) studies found values of 379 and 284 meV for the C−H and C−D stretch modes of pyridine and pyridine-d_5 on Cu(110).[13] STM-IETS spectra on Cu(110) exhibit peaks at 379 and 281 meV.[11] Five C−H stretch modes exist for free pyridine over a range of ∼8 meV.[14] Because the width of the pyridine C−H stretch peak in Figure 1b is 17 meV, individual modes would not be resolved. The width of the acetylene C−H stretch, a single mode, is 14 meV. The larger width of the pyridine peak may therefore be due to the contribution of more than one tunneling-active mode.

The change in conductance due to the onset of inelastic tunneling is a useful quantity for comparing the relative probabilities of inelastic tunneling between tunneling-active modes. It is obtained by integrating d^2I/dV^2 over the peak areas and normalizing by the conductance dI/dV. The changes in conductance for the spectra in Figure lb are 5% for the C−H stretch of pyridine and 3.5% for the C−D stretch of pyridine-d_5. For comparison, the C−H and C−D modes of acetylene-d_1 give conductance changes of 7% and 5%. Though spectral differences exist between pyridine and pyridine-d_5 at other energies, additional vibrational peak assignments cannot be made at this time. The feature near 210 meV is specific to the electronic structure of the tip used to take the spectra.

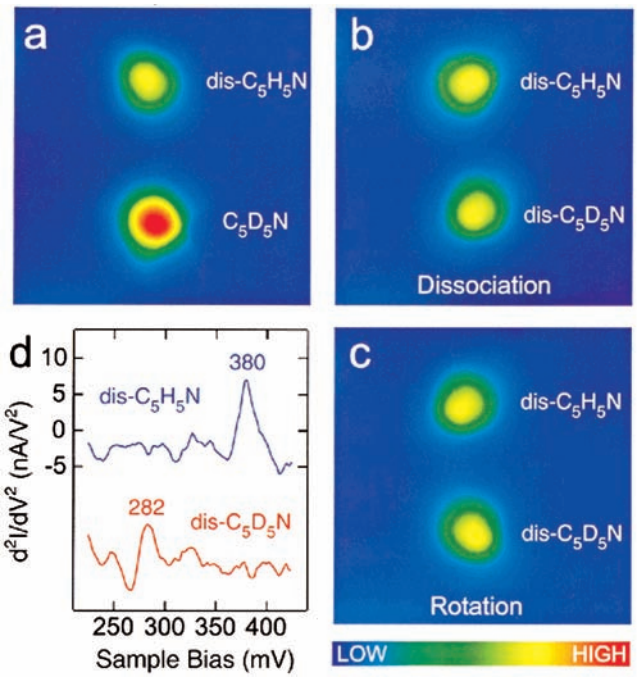

Figure 2. (a) 44 × 44 Å image of pyridine-d_5 (lower) and a pyridine dissociation product with the same tip and imaging conditions as in Figure 1. The asymmetry in the pyridine-d_5 image is due to the tip shape. (b) Dissociation product of pyridine-d_5 (lower) and the pyridine fragment of (a) rotated 90° cw. (c) The upper fragment rotated 180° and the lower 90° ccw. (d) Background-subtracted d^2I/dV^2 spectra for the fragments in c. The spectra are averages of 40 scans using the same gap resistance, modulation voltage, voltage increment, and averaging time per point as the spectra shown in Figure 1b.

Pyridine Dissociation. Dissociation was carried out by positioning the tip over the molecule to be dissociated, turning off the feedback, and retracting the tip a distance which, when the voltage was increased, resulted in a 1 nA tunneling current. Pyridine dissociation was accompanied by a sudden drop in the tunneling current, at which point the voltage was returned to the scanning bias of 0.25 V and the feedback turned on. An image was then taken to confirm that dissociation had taken place and to view the reaction products. The threshold dissociation voltage depended on the tip,[15] but typical dissociation voltages observed for pyridine and pyridine-d_5 were 3.0 ± 0.1 and 3.2 ± 0.1 V.

The primary dissociation step consistently resulted in a single fragment 70% reduced in height from the parent molecule (Figure 2a). The fragment image has a single mirror plane and is therefore of C_s symmetry. The four possible orientations of the fragment, shown in Figures 2a−c, demonstrate that this assignment reflects the symmetry of the molecule and not the tip. The mirror plane of the fragment is perpendicular to the surface, is parallel to the copper [110] or [1̄10] axis, and contains the axis of rotation. The axis of rotation of the fragment is displaced from the maximum of the parent molecule image a distance of 1.8 Å, or half the lattice spacing, in the [001] direction. Fragments were rotated by positioning the tip at the maximum of the image and tunneling at a 3 V sample bias.

STM-IETS was performed on the fragments of pyridine and pyridine-d_5 (Figure 2d). The position of the C−H (C−D) stretch mode of the fragment is shifted +3 meV (+1 meV) with respect to the parent molecule (Figure lb). The uncertainties in the peak positions are ∼1 meV. The peak widths of the fragment spectra

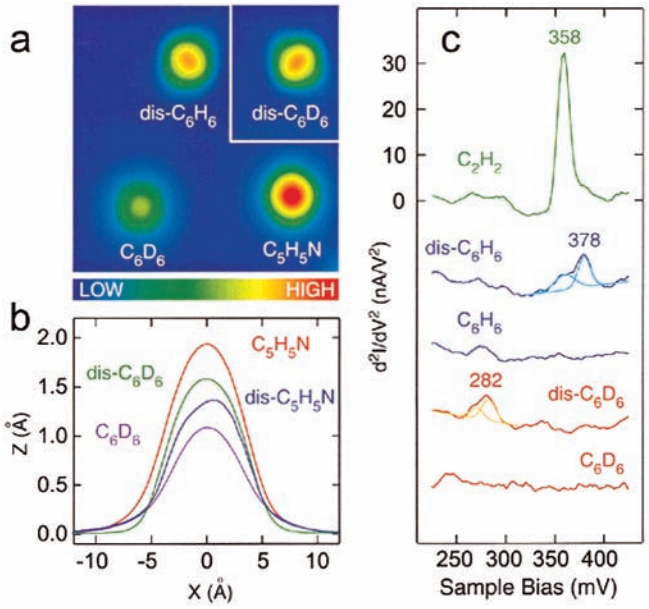

Figure 3. (a) 47 × 47 Å image of pyridine, benzene-d_6, and a benzene fragment. The inset shows another fragment rotated 90° from the orientation of the first. (b) Cross sections of benzene, pyridine, and fragments taken along the mirror planes of the molecules. The cross sections of largest width are shown. Pyridine and pyridine fragment cross sections are from Figure 2a. (c) Background-subtracted d^2I/dV^2 spectra for benzene isotopes and dissociation products with an acetylene spectrum for comparison. The spectra are averages of 100 scans using the same averaging time per point as previous spectra. The spectra were taken with the same gap resistance, modulation voltage, and voltage increment as the spectra of Figures lb and 2d but on a different day with a different tip. A slight change in the tip preceded acquisition of the C_6H_6 spectrum, giving rise to a small peak of electronic origin near 275 meV. Gaussian fitting curves for the fragment spectra are superposed.

are the same as those of the parent molecules. The relative changes in conductance are 4% for the C−H mode and 3% for the C−D mode.

Benzene. Benzene adsorbs associatively and parallel to the Cu(111) surface.[16] There is disagreement as to whether benzene adsorbs parallel[9,13,17] or tilted[18] with respect to the Cu(110) surface. Calculations of benzene adsorbed on Cu(001) have found a parallel physisorbed species with no significant structural distortions.[19] Figure 3a shows an image of pyridine, benzene-d_6, and a benzene fragment on Cu(001). Benzene fragments were produced in the same manner as the pyridine fragments. As with pyridine, the first dissociation step consistently led to a single observable reaction product. The minimum observed dissociation threshold was 2.9 ± 0.1 V for benzene and 4.4 ± 0.1 V for benzene-d_6. While the benzene dissociation event was local, the voltage necessary for benzene-d_6 dissociation was in the field emission regime and occasionally led to dissociation of nearby benzene. At voltages above 1.5 V, benzene could also hop away from the tip without dissociating. Dissociation was confirmed by imaging. The benzene fragments were usually displaced from the parent molecules, but dissociation events were noted in which the fragment image maximum coincided with that of the parent molecule. This indicates that benzene and its dissociation product can occupy the same adsorption site.

Cross sections for pyridine, benzene, and their dissociation products are shown in Figure 3b. The benzene fragment height with respect to the surface is 140% greater than that of benzene. Images of benzene on Cu(001) showed some indication of C_{4v} symmetry which may reflect the symmetry of the adsorption site. The fragment image possesses two mirror planes and is therefore of C_{2v} symmetry. The fragment is found in one of two orientations, shown in Figure 3a and the inset. The mirror planes are parallel to the copper [110] and [1$\bar{1}$0] axes. The reduced symmetry of the pyridine fragment with respect to the benzene fragment can be seen clearly in the fragment cross sections of Figure 3b.

Secondary dissociation of the pyridine and benzene fragments could be induced at voltages above 3.75 V. Unlike the first dissociation step, the second dissociation did not consistently produce the same reaction product. Two products were often produced, one of which imaged as a depression and one as a protrusion. This can be interpreted as a breaking of the π-resonant ring structure. The products of the second dissociation were not identified.

IETS spectra for benzene, benzene-d_6, and their fragments are shown in Figure 3c. A spectrum for acetylene is shown for comparison. No peaks are observed in the C−H stretch region for benzene, but the benzene fragment shows peaks that are assigned to C−H stretch modes based on the position and observed isotope shift. The onset of C−H stretch modes upon dissociation may be due to a reorientation of the ring plane from a parallel to inclined geometry. This possibility is discussed below in greater detail. The C−H peaks occur at 379 and 359 meV, and the C−D peaks occur at 282 and 270 meV. The changes in conductance associated with these modes are 3%, 2%, 2%, and 1%. The change in conductance for the acetylene C−H stretch mode is 12%.[20] For comparison, high-resolution electron energy loss spectroscopy (EELS) studies of benzene on Cu(110) revealed a C−H mode at 378 meV,[18] which is comparable to the higher energy peak. The peak widths are all 16 meV with the exception of the lower C−H peak, which has a width of 24 meV. The calculated error in fitting the peaks was ~1 meV, but systematic errors may be introduced by assuming the spectrum consists of two modes. Benzene, like pyridine, has more than one C−H stretch mode, so it is not suprising to find evidence of more than one mode in the benzene fragment which has even lower symmetry than the parent.

Discussion

The results of the STM imaging, dissociation, and spectroscopy studies presented here are best understood in light of previous studies of benzene and pyridine on transition and noble metal surfaces. Benzene adsorbs with its molecular plane parallel to the surface on many metal surfaces.[13,17,21−23] Bonding to the surface is primarily through the delocalized π-electron system. Pyridine, which has a nitrogen atom substituted for a benzene C−H group, may bond to the surface either through the π electrons or through the lone pair of electrons associated with the N atom. The relative contribution of N lone pair and π bonding depends on the surface, temperature, and coverage. The angle between the surface and the pyridine molecular plane increases as the bonding through the nitrogen increases. The angle may also be changed by varying the potential of the adsorption surface in an aqueous solution.[24] On Cu(110), pyridine bonds to a single copper atom through the nitrogen and the molecular plane is perpendicular to the surface and the [1$\bar{1}$0] close-packed axis.[9,10] On Pd(111) at 180 K, pyridine adsorbs parallel to the surface but becomes tilted as the temperature increases along with the nitrogen bonding.[23] On Pt(111)[13,25] and Ni(001)[22] below 240 K, pyridine shows mixed π and N lone pair bonding. As the temperature is increased above 240 K [260 K] for Ni(001) [Pt(111)], pyridine either desorbs or converts to α-pyridyl (C_5H_4N) through the loss of

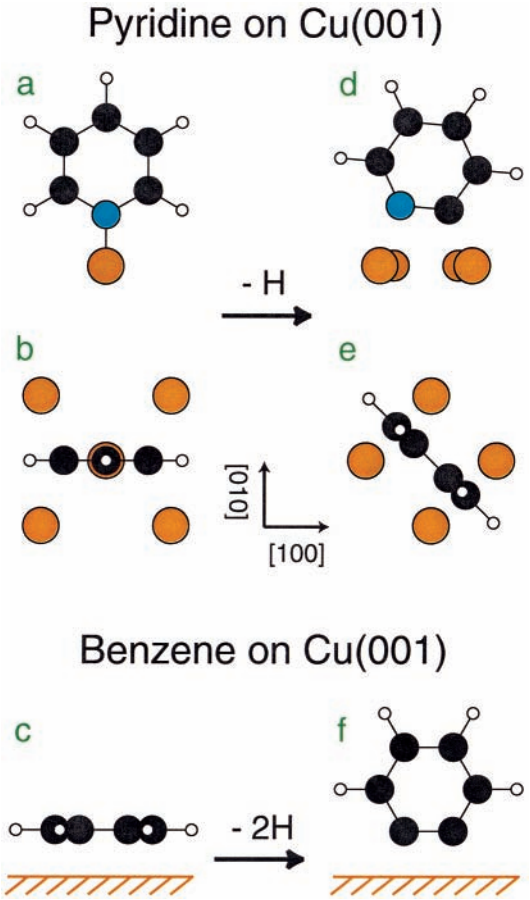

Figure 4. Adsorption geometries for pyridine (a, b) and benzene (c) on the Cu(001) surface. a and c are side views; b is a top view. The azimuthal orientation of pyridine (b) was chosen based on the observation of the molecular plane being perpendicular to the close-packed rows on the Cu(110) surface in ref 9. (d−f) The proposed tunneling electron induced dissociation products and their orientations with respect to the surface. The view of d is along the [110] axis, and the copper atoms in e are shifted $^1/_2$ lattice constant from those of b to reflect the new binding site. The azimuthal orientation of the ring plane for the pyridine product (e) is based on the imaging evidence. The azimuthal orientation of the ring plane for the benzene product is the same as that of pyridine, but the binding site was not determined. The symmetry of the STM images indicates the on-top or four-fold hollow site. The orientation of the Cu(001) surface was determined by high-resolution images of acetylene; the acetylene mirror planes are parallel to Cu(100) and Cu(010).

one hydrogen adjacent to the nitrogen atom (the α-H). Similar behavior is seen on Ru(001).[10] α-Pyridyl is found to bond with the ring structure perpendicular to the surface on Ni(100) and Ru(001).

Concomitant with an increase in the molecule−surface angle are changes in the intensities of various vibrational modes observed by EELS and RAIRS. In EELS studies, for example, the specular intensity of in-plane modes increases and the intensity of out-of-plane modes decreases as the molecule tilts upward because of the dipole selection rule.[23] Upon conversion of pyridine to α-pyridyl, the C−H mode energy shifts upward by 1−8 meV depending on the surface.[10,22,25]

On the basis of our STM data and the previous work mentioned above, we propose that the pyridine reaction product is α-pyridyl and the benzene reaction product is C_6H_4 (Figure 4). The evidence is not conclusive but suggestive. Three types of evidence led to this assessment: the isotopic dependence of the benzene dissociation threshold, the symmetries of the molecular images, and the inelastic tunneling spectra.

Isotopic Evidence. The large isotopic difference in dissociation threshold bias for benzene suggests that the C−H and C−D bonds are being broken; these are the bonds which are most affected by the isotopic substitution. The isotopic difference is smaller in pyridine. This could be indicative of a different dissociation mechanism. Photodissociation of pyridine and benzene reveals notable differences between the two molecules. In the photodissociation of benzene by 193 nm light, 96% of the dissociation events result in the loss of one or two hydrogen atoms.[26] Pyridine, in contrast, loses a hydrogen in only 9% of events. The remaining percentage consists of events which result in the destruction of the ring structure.[27] It was mentioned above, however, that the thermal dissociation of pyridine on several surfaces always results in α-H−C bond cleavage. The changes induced by chemisorption may make this pathway facile for dissociation by tunneling electrons as well.

Imaging Evidence. The fragments have the same surface point group symmetries as the proposed reaction products. The pyridine fragments of Figure 2a−c are of C_s symmetry with the mirror plane found along the [110] or [1$\bar{1}$0] Cu axes. The fragment can be assigned to a binding site of four-fold symmetry based on its four equivalent orientations. Assuming pyridine is bound upright to a copper atom through the nitrogen lone pair, analysis of Figure 2a−c suggests that the pyridine fragment is centered on a four-fold hollow site. The fragment symmetry is consistent with the pyridine losing an α or β hydrogen with no change in orientation. The same symmetry could be obtained by losing an α, β, or γ hydrogen and rotating the molecule about an axis perpendicular to the ring. Considerations of steric hinderance make a rotation without the loss of an α-H implausable. A tilting of the ring plane toward the surface is ruled out by the symmetry of the fragment images. The α-pyridyl species, which bonds with the molecular plane perpendicular to the surface and tilts to allow α-C to participate in bonding, is consistent with the fragment images.

The benzene fragment shown in Figure 3a is of C_{2v} symmetry with mirror planes along the copper [110] and [1$\bar{1}$0] axes. There are two equivalent orientations, 90° apart. This is consistent with the symmetry of C_6H_5 or C_6H_4 bonded to the surface through the dehydrogenated carbon atom(s) and centered on a site of four-fold symmetry. The ring plane would be parallel to the copper [110] or [1$\bar{1}$0] axes and perpendicular to the surface. The C_6H_4 seems more plausible considering the lack of C_{2v} symmetry in the C_6H_5N image and the presence of C_{2v} symmetry in the benzene fragment image. The substitution of N for C in C_6H_5, however, could change the molecular orbitals involved in tunneling and therefore affect the appearance of the image.

The relative heights of the fragments, shown in Figure 3b, must be analyzed with caution as the corrugation of STM images is primarily an electronic, not geometric, effect. The geometrical changes in molecular orientation caused by dissociation are accompanied by changes in the electronic structure, both of which affect the height and shape of the images. It is reasonable to assume, however, that the height difference between pyridine and benzene is, in part, due to the difference in adsorption geometry and is not a purely electronic effect. Analogously, a perpendicularly bonded species of benzene should appear taller than a parallel species. If the bonding of C_6H_5 and C_6H_4 is similar to that of pyridine and α-pyridyl, one would expect these benzene fragments to be bonded perpendicular to the surface and hence taller than the benzene in constant current images. Accurate calculations of the bonding geometries of these fragments coupled with STM image simulations could be performed to confirm this. The relative height difference

between pyridine and the proposed α-pyridyl fragment could be both geometrical and electronic in origin. The molecular height is reduced when the molecule tilts in-plane to form a di-σ bond between the copper and the C and N atoms. The height difference between pyridine and benzene fragments is also likely to be of dual origin as the Cu−C and Cu−N bonds should differ in length and energy. Calculations of the structures and energies of these different species and STM studies with other isotopes can further our understanding of these systems.

Spectral Evidence. The C−H stretch peak of the pyridine fragment is 3 meV higher than that of pyridine. The C−D stretch peak of the pyridine-d_5 fragment is 1 meV higher than that of pyridine-d_5. A similar upshift in energy is seen upon thermal conversion of pyridine to α-pyridyl on the Ru(001),[10] Ni(100),[22] and Pt(111)[13,25] surfaces. In a study of benzene, pyridine, and α-pyridyl on Ni(100),[22] the benzene and pyridine C−H stretch energies were the same whereas the α-pyridyl energy was 7 meV higher. The loss of hydrogen in pyridine results in an upshift of the C−H stretch energy, and the same could be true for benzene. C_6H_4, however, should not be expected to have the same mode structure as C_5H_4N; the substitution of N for C−H results in additional modes and altered excitation cross sections.

The lack of a C−H stretch mode in STM-IETS spectra of parallel benzene and the presence of C−H stretch modes in the presumed perpendicular benzene fragment are analagous to the onset of the in-plane C−H stretch of pyridine noted in EELS when the pyridine is tilted up by heating.[23] In addition, the fragment spectra show at least two C−H modes of different intensities. Selection rules have not been established for the tunneling-active modes seen in STM-IETS; experiments of this kind are necessary to their determination in the absence of a predictive theory.

Implications

One of the aims of this paper is to illustrate the myriad of ways in which the STM can study the adsorption and unimolecular reaction of unsaturated six-membered ring molecules. The STM can be used to induce a chemical reaction and characterize the initial and final states on the atomic scale. The implications of the information gained by these methods to a general understanding of chemical and biological systems are summarized below.

Single-Molecule Vibrational Spectroscopy. STM-IETS is a promising technique that can produce a mapping of vibrational excitations within a molecule in addition to providing spectroscopic information.[6,28] The observation reported here of the appearance of a tunneling-active mode due to a change in bonding geometry is one step toward understanding the mechanisms underlying STM-IETS and extending the technique to more complex adsorption systems. For example, several biologically important molecules are constituted of entities similar to benzene and pyridine. The structural configuration of these subunits may affect their observability via STM-IETS. In addition, any useful theory of STM-IETS will need to account for the effects of adsorbate geometry on the inelastic tunneling cross section.

Electronic Structure Calculations. A rigorous theoretical account of the experimental results detailed here would include the prediction of molecular reorientation and bonding site shift upon partial dehydrogenation. The changes in electronic structure which contribute to the differences in apparent height and vibrational spectra are also of interest. Benzene and pyridine provide a useful test of calculations as they are structurally quite similar but can exhibit very different behaviors. The correct calculation of adsorption sites is an important goal of theory because the adsorption site is often crucial to the catalytic activity of a surface. The detailed, quantitative geometrical information provided by STM images and the corresponding theoretical interpretation can contribute to our understanding of chemistry on the microscopic scale.

Atomic Scale Chemistry. The breaking of a single bond is not a simple event. The dynamical evolution of charge distribution induced by the tunneling of an energetic electron into a molecule is affected by the interplay between the motions of electrons and nuclei and the transfer of energy between them. A complete picture emerges when one is able to understand how the redistribution of energy on the molecular scale results in bond breaking or bond formation. The STM is able to initiate such changes and study the results with atomic precision.

Acknowledgment. This research was supported by the National Science Foundation under Grant DMR-9417866 and through a NSF Traineeship (L.J.L.). In addition, W.H. thanks William A. Goddard, III, for insightful discussions on the nature of the chemical bond.

References and Notes

(1) Chiang, S. *Chem. Rev.* **1997**, *97*, 1083.
(2) Weiss, P. S.; Eigler, D. M. *Phys. Rev. Lett.* **1993**, *71*, 3139.
(3) Sautet, P.; Bocquet, M.-L. *Surf. Sci.* **1994**, *304*, L445.
(4) Avouris, Ph. *Acc. Chem. Res.* **1995**, *28*, 95.
(5) Stipe, B. C.; Rezaei, M. A.; Ho, W. *Phys. Rev. Lett.* **1997**, *78*, 4410. Stipe, B. C.; Rezaei, M. A.; Ho, W. *J. Chem. Phys.* **1997**, *107*, 6443.
(6) Stipe, B. C.; Rezaei, M. A.; Ho, W. *Science* **1998**, *280*, 1732.
(7) Stipe, B. C.; Rezaei, M. A.; Ho, W. *Rev. Sci. Instrum.* **1999**, *70*, 137.
(8) Bandy, B. J.; Lloyd, D. R.; Richardson, N. V. *Surf. Sci.* **1979**, *89*, 344.
(9) Bader, M.; Haase, J.; Frank, K.-H.; Ocal, C.; Puschmann, A. *J. Phys.* **1986**, *47*, C8−491.
(10) Bridge, M. E.; Connolly, M.; Lloyd, D. R.; Somers, J.; Jakob, P.; Menzel, D. *Spec. Chim. Acta* **1987**, *43A*, 1473.
(11) Lauhon, L. J.; Ho, W., unpublished results.
(12) In all measurements, the root mean square (rms) value of the modulation is reported, and the voltage is that of the sample with respect to the tip.
(13) Haq, S.; King, D. A. *J. Phys. Chem.* **1996**, *100*, 16957.
(14) Wiberg, K. B.; Walters, V. A.; Wong, K. N.; Colson, S. D. *J. Phys. Chem.* **1984**, *88*, 6067.
(15) For the purposes of this discussion, the dissociation threshold is defined as the minimum observed voltage which produced dissociation within 10 s at a 1 nA tunneling current.
(16) Xi, M.; Yang, M. X.; Jo, S. K.; Bent, B. E.; Stevens, P. *J. Chem. Phys.* **1994**, *101*, 9122.
(17) Doering, M.; Rust, H.-P.; Briner, B. G.; Bradshaw, A. M. *Surf. Sci. Lett.* **1998**, *410*, L736.
(18) Lomas, J. R.; Baddeley, C. J.; Tikhov, M. S.; Lambert, R. M. *Chem. Phys. Lett.* **1996**, *263*, 591.
(19) Triguero, L.; Pettersson, L. G. M.; Minaev, B.; Ågren, H. *J. Chem. Phys.* **1998**, *108*, 1193.
(20) With the same tip and tunneling conditions, the C−H stretch signal of acetylene (C_2H_2) is twice as large as that of acetylene-d_1 (C_2HD).
(21) Bertolini, J. C.; Rousseau, J. *Surf. Sci.* **1979**, *89*, 467.
(22) DiNardo, N. J.; Avouris, Ph.; Demuth, J. E. *J. Phys. Chem.* **1984**, *81*, 2169.
(23) Grassian, V. H.; Muetterties, E. L. *J. Phys. Chem.* **1987**, *91*, 389.
(24) Cai, W.-B.; Wan, L.-J.; Noda, H.; Hinibo, Y.; Ataka, K.; Osawa, M. *Langmuir* **1988**, *14*, 6992.
(25) Grassian, V. H.; Muetterties, E. L. *J. Phys. Chem.* **1986**, *90*, 5900.
(26) Yokoyama, A.; Zhao, X.; Hintsa, E. J.; Continetti, R. E.; Lee, Y. T. *J. Chem. Phys.* **1990**, *92*, 4222.
(27) Prather, K. A.; Lee, Y. T. *Isr. J. Chem.* **1994**, *34*, 43.
(28) Stipe, B. C.; Rezaei, M. A.; Ho, W. *Phys. Rev. Lett.* **1999**, *82*, 1724.